ACQUISITION, PROCESSING AND INTERPRETATION OF THE LALOR 3C-3D SEISMIC DATA

GILLES BELLEFLEUR[1], ERNST SCHETSELAAR[1], AND DON WHITE[1]
[1] *Geological Survey of Canada, 615 Booth Street, Ottawa, Ontario, K1A 0E9*

INTRODUCTION

During the winter of 2013, the Geological Survey of Canada acquired a 16 km^2 3-component 3D seismic data set over the Lalor volcanogenic massive sulphide deposit located in Manitoba, Canada (Figure 1) to assess the reflectivity of the ore and further validate the potential of 3D reflection seismic methods for deep mineral exploration. In this section, we present the main field acquisition and processing parameters. Results presented here based on only P-wave processing of the data recorded on the vertical component of the receivers. Finally, we analyze and interpret the main reflections associated with the hanging wall, ore zones, and footwall, and use this information to provide guidelines for the exploration of similarly metamorphosed massive sulphide deposits.

DATA ACQUISITION AND PROCESSING

The 3D active-source seismic survey covers an area of approximately 16 km^2 that includes 908 shot points and 2685 receiver stations (Figure 1). The 16 receiver lines were oriented SW-NE and are almost parallel to the dip direction of the ore zones and footwall rocks near the deposit. The 15 shot lines were generally orthogonal to the receiver lines with many shot points located northeast of the deposit to provide sufficient ore zone illumination from the down-dip direction. Shot and receiver lines locally deviated from planned location to adjust for difficult terrain (e.g., steep hills, cliffs). Deviations were more significant logistically for shot lines which provided access for the track-mounted drill rigs used for the shot holes. The area between Lalor Lake and Cook Lake was particularly challenging for shot lines (Figure 1). No shots were fired close to existing mining infrastructure including the main mine area and ventilation raise, or over lakes (Figure 1). Energy sources were 0.5 kg of explosives loaded in 5 m deep holes that were tamped with bentonite and cuttings from the drilling. Digital multi-component accelerometers deployed at 2685 stations were kept live for the entire survey (i.e., one receiver patch was used) and provided a total of 8055 traces per shot gather. The generally cold temperatures during the 3D acquisition (generally below minus 20^o C during the acquisition phase in March 2013) resulted in solidly frozen near-surface conditions, which allowed excellent ground-to-geophone coupling. Table 3 shows the main acquisition parameters used for the 3D seismic data acquisition.

The quality of the raw shot gathers ranges from poor to excellent with most shot gathers generally having good signal-to-noise ratio and clear first arrivals at large offsets (up to 4 km). Many of the poor-quality shot gathers are located in areas with muskeg that strongly reduces the shot coupling and attenuates seismic waves. Figure 13a shows a typical raw shot gather recorded on receiver lines 133 to 141 (Figure 1 for location). Direct, refracted P-waves, S-waves, and surface waves are the most prominent arrivals on the shot gather. Weak and mostly discontinuous reflections are occasionally identified on raw shot gathers. Much of the surface wave energy on the shot gather is characterized by frequencies typically below 45 Hz. The best shot gathers have signal at frequencies up to 250 Hz whereas signal on poor-quality shot gathers only reaches 100 Hz. However, average shot records have high amplitudes (i.e., within 10 dB of the maximum amplitude) at frequencies ranging between 150-200 Hz.

Table 3. Acquisition parameters for the 3D-3C Lalor seismic survey.

Sensor/accelerometer	Sercel 428/DSU3 (3C)
Traces/record	3 x 2685
Sample interval	1 ms
Sample /trace	4001
Anti-alias filter	400 Hz
Source type/ Source depth	0.5 kg explosive / 5m
No. of shots	908
Source spacing/line spacing	50 m/ 365 m
Receiver spacing/line spacing	25 m/ 250 m
No. of source/receiver lines	15/16
Patch	All live
Survey area	16 km^2

The final seismic images presented in this paper were obtained using a prestack dip-moveout (DMO) and poststack time migration processing flow. Such a processing flow is particularly effective and often produces superior results to images obtained with prestack-time migration for seismic data acquired in crystalline rock environments (Milkereit *et al.*, 1996; Adam *et al.*, 2003; White *et al.*, 2012). The stacked DMO volumes also preserve diffractions that may originate from smaller ore bodies, edges or larger massive sulphide lenses (Malehmir and Bellefleur, 2009). At Lalor, results from this approach produced generally more continuous reflections with significantly less short and discontinuous reflections than did a trial prestack-time migration processing flow. The number of short and discontinuous reflections is particularly significant in the shallow part of the prestack-time migrated volume and the great majority could not be reconciled with observed geological features

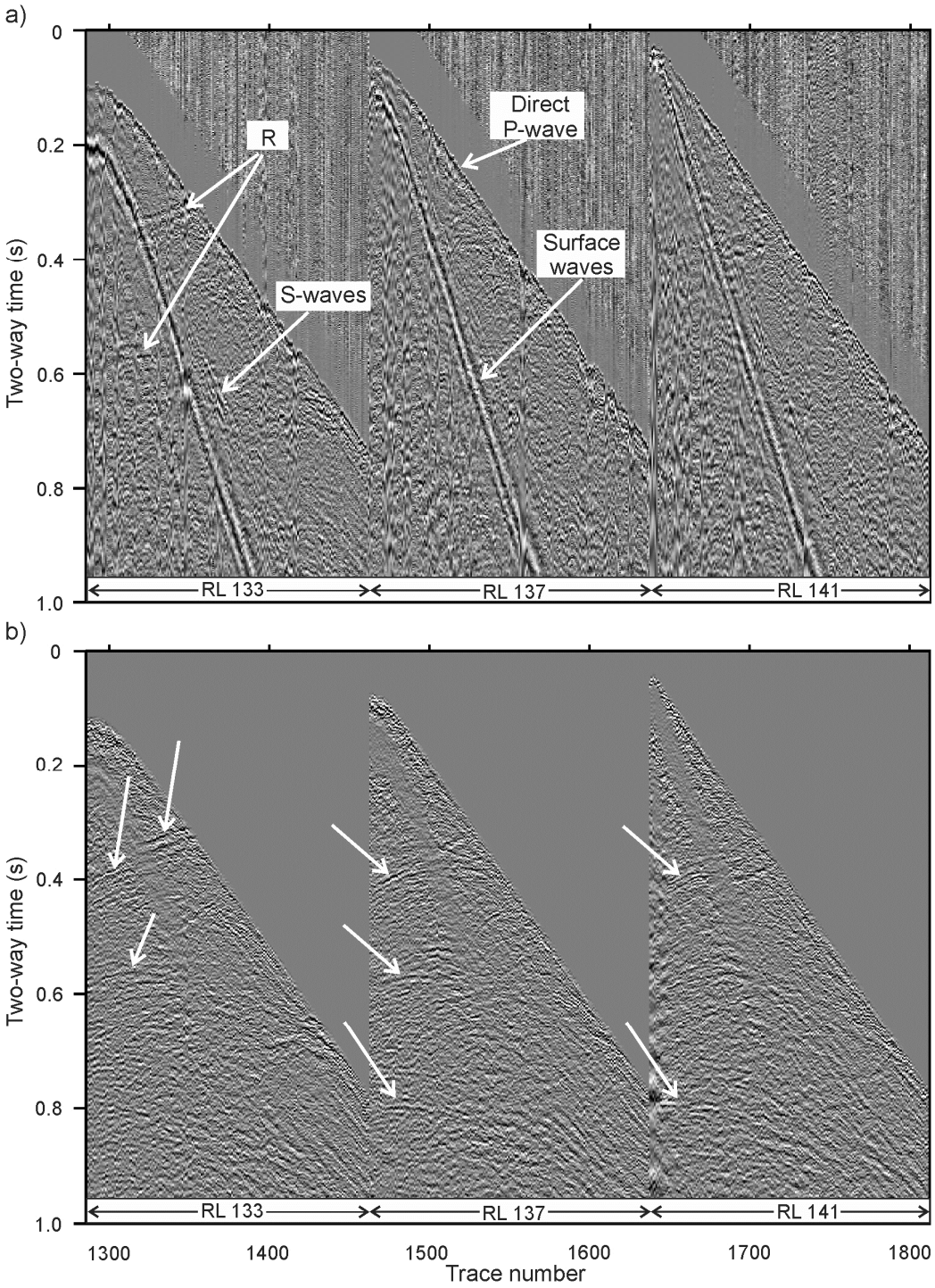

Figure 13. (a) Example of a good quality raw vertical-component shot gather (FFID 224; see Figure 1 for location) on three receiver lines. (b) Same shot gather after some processing (refraction static corrections, coherent noise attenuation and surface- consistent deconvolution). Arrows point to a few reflections (R in a).

Table 4. Processing parameters for the prestack DMO poststack migration flow.

Step	Parameters
1.	Geometry assignment and 3D Binning, CDP Bin size 12.5 m x 25.0 m
2.	Trace editing
3.	Trace balancing (2 second window)
4.	Spherical divergence correction
5.	Refraction static corrections, datum = 330 m, Vr = 5900 m/s
6.	Spiking deconvolution 80 ms filter length
7.	F-k filter on shot and receiver gathers to attenuate surface and refracted arrivals
8.	Air wave removal
9.	Band pass filter 5-35-175-225 Hz
10.	Automatic Gain Control, 500 ms window length
11.	Velocity analysis (iterative)
12.	Surface-consistent residual statics, max shift 15 ms, window 200-1500 ms (iterative)
13.	Normal moveout correction
14.	Dip moveout correction – 3D integral method (iterative - 3 loops)
15.	CDP trim statics, max shift 8 ms
16.	Stacking
17.	3D Kirchoff poststack time migration
18.	Automatic Gain Control, 300 ms window length
19.	Band pass filter 10-35-160-190 Hz
20.	Curvelet denoising

near the deposit. However, both processing approaches revealed the stronger and most continuous reflections. Results from the prestack-time migration processing flow can be found in Bellefleur and White (2014). Table 4 shows the detailed sequence and parameters used to process the vertical-component of the Lalor 3D data presented in this paper (prestack DMO-poststack migration processing flow).

Of the pre-processing steps (see Table 4), trace editing and coherent noise attenuation were particularly important steps. Noisy traces with no clear first arrivals and weak traces contaminated with occasional mining noise were removed during trace editing. When present, the strong mining noise typically formed sequences of coherent hyperbolic arrivals randomly distributed in time, including before the first arrivals. The apexes of the hyperbolic events were always located at receiver stations near the main mining area. Traces with such noise were removed from the data. The main underground explosions occurred twice a day at times communicated by the mine personnel and were avoided by temporarily stopping recording during data acquisition.

Approximately 6.5% (162429 traces) of the traces were eliminated during trace editing. Refracted shear-waves and surface waves were attenuated with 2D filtering in the frequency-wavenumber domain combined with a bandpass filter (5-35-175-225 Hz). Some refracted S-waves still remained after these steps and were further attenuated using median filters that followed a linear moveout velocity of 3200 m/s. Refraction and elevation static corrections were instrumental in improving the continuity of reflections in shot gathers (Figure 13b). The 3D refraction static corrections were determined from over 1.2 million picked arrivals. An automatic picking algorithm combined with manual inspection and adjustments were used to pick the first arrivals. Receiver refraction statics varied from -6 ms to 46 ms with most receivers being within the -3 to 7 ms range. The largest receiver static corrections were located over Cook Lake (Figure 1). Shot statics were generally smaller and ranged between -4 and 21 ms with a mean of 3 ms.

The pre-processed data were then sorted into common depth point gathers using a bin size of 12.5 m by 25 m in the inline and crossline directions, respectively. Nominal fold reached a maximum of 170 in the centre of the 3D grid. Three iterative loops of NMO-DMO were used to update the velocity models. Residual static corrections were included in the last two NMO-DMO loops. A 3D Kirchhoff poststack time migration was applied to the final DMO stack volume. Post-migration filtering included an automatic gain control (300 ms window), bandpass filter (10-35-160-190 Hz), and curvelet denoising. Curvelet denoising provided a higher signal-to-noise ratio than did F-XY deconvolution which is often applied as a post-migration filter (Górszczyk *et al.*, 2015). The final time-migrated volume was converted to depth using a constant velocity of 5900 m/s and then integrated with the 3D geological model. This velocity is supported by borehole logging data, particularly in the hanging wall and produced the most satisfactory tie with borehole data (see Bellefleur *et al.*, 2015).

DATA INTERPRETATION

Hanging Wall Reflections

The final seismic data are compared with the geological model in Figures 10 and 12. The hanging wall is generally devoid of reflections mostly due to the near-vertical orientation of strata in the hanging wall. This is especially the case above the deposit where reflections are generally short and weak, and have no obvious correlation with lithological units (Figures 10 and 12). Some weak shallowly-dipping reflections are observed towards the northeast end of the model (H1 to H3 on Figure 14) where hanging wall units have shallower dips in the 3D geological model. Reflection H2 on Figure 14 is located at the contact between mafic volcanic and mafic volcaniclastic rocks. The mafic volcaniclastic unit just above the hanging wall- footwall contact has relatively high density values that could potentially explain the reflections even though such an increase in density is not associated with a clear reflection on the synthetic trace (see Bellefleur *et al.*, 2015). Reflections H1 and H3 are observed within a felsic or mafic volcanic unit and cannot be explained due to lack of borehole constraints near the northeastern edge of the model. Some short sub-horizontal

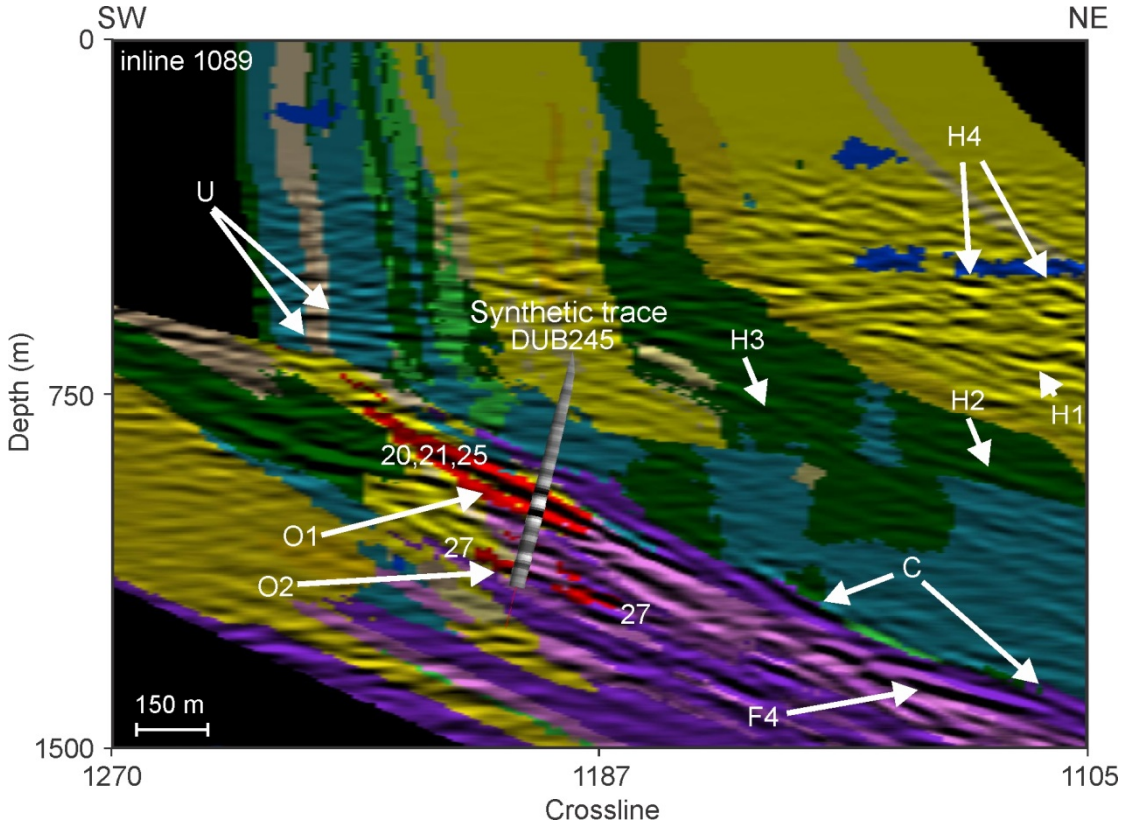

Figure 14. Inline 1089 from the final migrated seismic volume with the geological model overlain on top of the seismic section. See text for details on interpretation. Legend for geology as in Figure 5. The labels are referred to in the text. Ore zones 20, 21, 25, and 27 are also shown.

reflections are locally correlated with diorite intrusions (H4 on Figure 14). However, not all diorites intersected in boreholes have reflections associated with them (see other diorites in Figure 14). Overall, hanging wall reflections are not particularly significant in the area of the 3D model.

Some reflections with moderate amplitudes are observed further to the northeast outside the limits of the 3D geological model (Figures 11 and 12). The dip of these reflections is generally shallow (approximately 25°) and similar to the dip of reflections in the footwall. Whereas the exact cause for these reflections cannot be precisely assessed due to lack of borehole control, the surface geological map and the projection of lithological unit from the model help to define their nature. In particular, reflection H5 (Figure 15) is associated with or coincides with the continuity of a contact between felsic and mafic volcanic rocks. Reflection H2 shown in Figure 14 also continues to the northeast on inline 1098 (Figure 16a). Reflections H6 and H7 are observed in the northeast part of the seismic volume (Figures 11 and 12). Reflection H6 is interpreted as the continuity of a felsic-mafic contact between the Balloch basalt and North-Balloch rhydacite (see Figure 16). If true, then reflection H7 appears to coincide with the top of the North-Balloch rhyodacite. Detailed surface geological maps indicate the presence of a mafic volcaniclastic unit northeast of the North-Balloch rhyodacite (Bailes *et al.,* 2013). The contact between this unit and the North-Balloch rhyodacite may explain reflection H7.

Reflectivity along the hanging wall-footwall contact depends on the composition of units juxtaposed at the interface, footwall alteration, and the presence of mineralization, all of which vary spatially. On inline 1089 (Figure 14), this contact has no clear seismic signature with only a few short reflections being locally observed (event C on Figure 14). On the time slice, there are no clear reflections associated with the contact (Figure 15). However, the contact is clear and continuous on an east-west section (C on Figure 16b) where mafic units in the hanging wall are juxtaposed with felsic units in the footwall. The contact is also locally observed on inline 1098 (C on Figure 16a).

Ore Zones Reflections

Whereas physical properties alone suggest an easy distinction between semi- to massive sulphides and host rocks, the reality is complicated by the close proximity of several mineralized zones and their generally small thickness. For instance, clear reflections are observed at the location of the shallower ore zones on inline 1089 (O1 on Figure 14). Three ore zones (20, 21, and 25) are all comprised in the shallowest ore interval shown in red in the model and indicated by O1 on Figure 14. The reflections

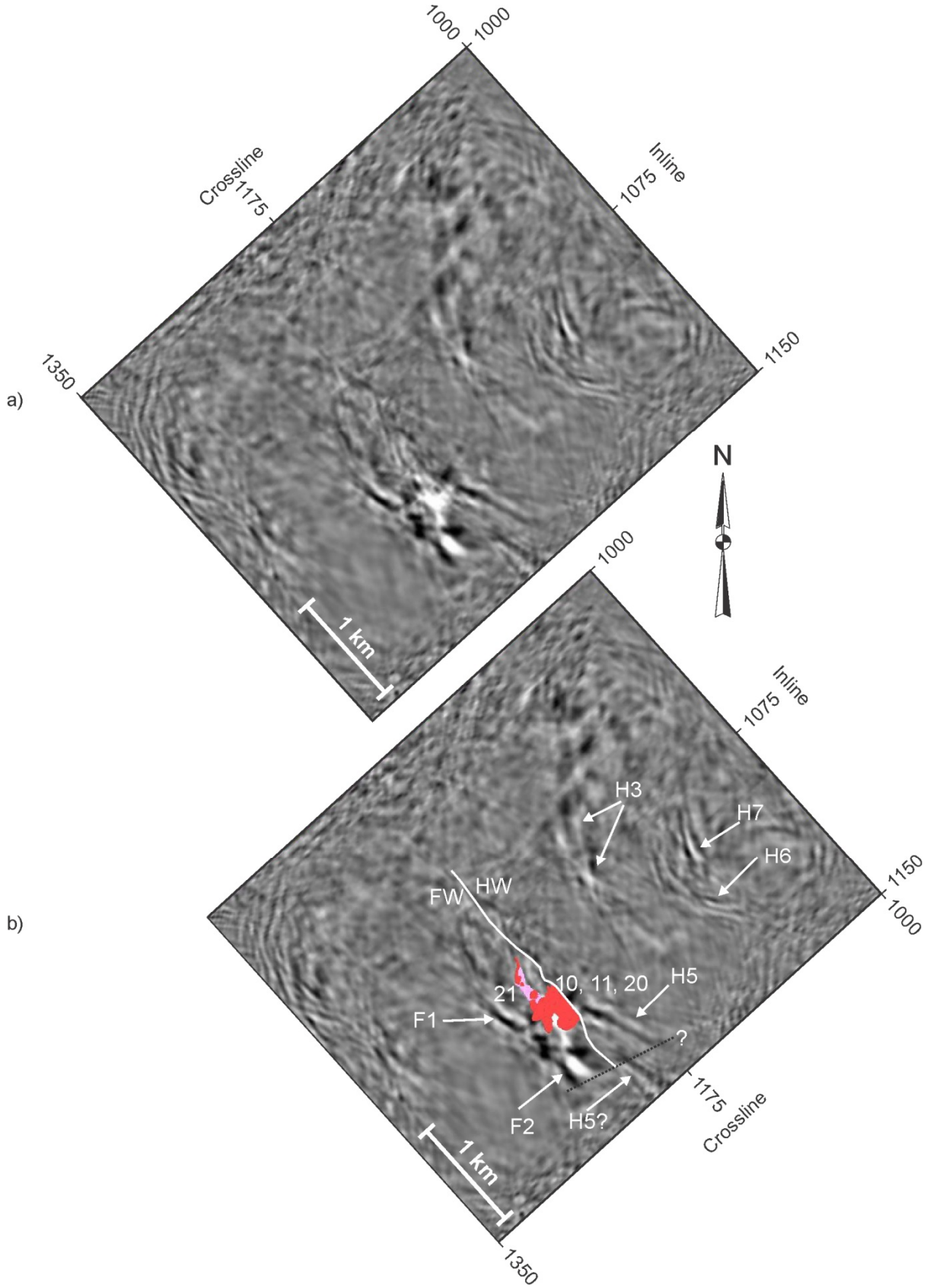

Figure 15. (a) Time slice at 283 ms (approximately 835 m depth) showing a strong amplitude anomaly at the location of the massive sulphide ore zones. (b) Same as (a) with interpretation. Ore zones 10, 11, 20 and 21 are shown in (b). Black dashed line indicates a possible fault.

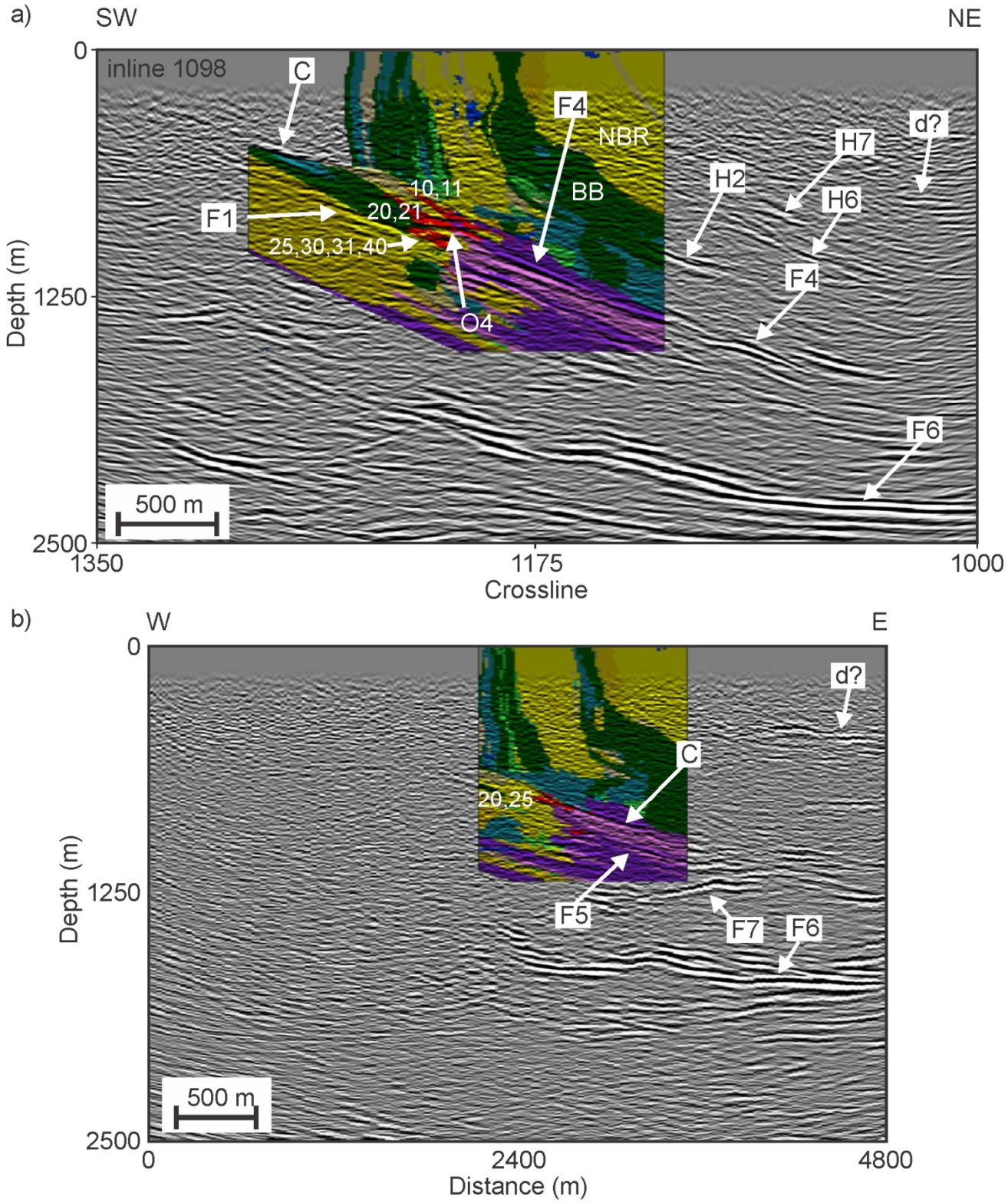

Figure 16. (a) SW-NE section (inline 1098) from the final seismic volume with geological information from the 3D model. (b) E-W section from the final seismic volume. The location of this E-W section is shown in Figure 1. See text for interpretation of events identified in (a) and (b). Legend for geology as in Figure 5. Post-migration curvelet denoising is not applied on these sections. Location of the cross-section is shown in Figure 1. Ore zones 10, 11, 20, 21, 25, 30, 31, and 40 are shown in (a). Ore zones 20 and 25 are shown in (b). BB: Balloch basalt; NBR: North-Balloch Rhyodacite.

result from the combination of the response of the shallow ore zone (zone 20) and contacts between felsic volcanic rocks and mafic protoliths above and below the ore zones (see also Bellefleur *et al.*, 2015). This combined effect is also observed on a time slice at 283 ms which correspond to a depth of approximately 835 m (Figure 15). The particularly strong localized amplitude anomaly on this time slice coincides with several ore zones (zones 10, 11, 20, and 21). The amplitude anomaly is clear and would have been identified as a potential target if the data would have been acquired as part of an exploration program. The deeper ore zone intersected in DUB245 (gold-copper zone 27) is indirectly associated with a reflection located at the contact between felsic and mafic protoliths (O2 on Figure 14). This reflection follows the felsic-mafic protolith contact on either side of zone 27. Other reflections are associated with ore zones elsewhere in the final seismic volume but those are not as strong as reflection O1 (see O3 and O4 on Figures 10 and 12). A series of sub-horizontal reflections coincide with ore zones 10, 20, 30, 31, and 40 on inline 1098 (Figure 16). The disseminated gold zones and gold-copper zone 27 have no clear reflections associated with them.

Footwall Reflections

In general, the number and strength of reflections are significantly higher in the footwall and especially in the intensely altered zone. On Figure 14, the less altered rocks in the immediate footwall are in general southwest of the main ore zones (units in yellow and green) whereas the most altered footwall rocks are southeast of the deposit (units shown in pink to purple). The strongest reflections in the least altered part of the footwall correspond to contacts between felsic and mafic volcanic rocks. Reflections from such contacts are observed on the time slice (F1 and F2 on Figure 15), and on inline 1098 (F1 on Figure 16a). Reflections in the most altered part of footwall are relatively continuous and can be tracked over significant distances, mostly to the northeast in the down-dip direction. These reflections coincide primarily with contacts between rocks with felsic and mafic protoliths. The correspondence between strong footwall reflections and felsic-mafic protolith contacts is clear in Figures 10 and 12 (see F4 and F5 on those figures). Figure 16b shows a strong sub-horizontal reflection just below the limit of the geological model (F7 on Figure 16b). This reflection merges with the felsic-mafic protolith reflection F4 approximately 500 m east of the area with geological information. The nature of this strong reflection cannot be established due to the lack of boreholes, but we speculate that it marks the bottom of the mafic protolith unit located above (F5 on Figure 16 is at the top of this mafic protolith unit). If so, the lithological unit below F7 would have a felsic composition or felsic origin (i.e., felsic protolith). At greater depths, the footwall is characterized by numerous reflections generally dipping to the northeast on most inlines (see F6 on Figure 16). The most continuous are located near the base of the Lower Chisel sequence near the contact with the Anderson sequence. Given their strength and excellent continuity, these reflections are likely of lithological origin but their exact nature still needs to be determined. Possibilities include the contact between the Chisel and Anderson sequences, a conformable mafic intrusion, and the continuation at depth of the synvolcanic Richard Lake pluton located west-to-southwest of the survey area. Based on the similarities in geometry of most footwall reflections (see Figure 16a), we infer that the deeper reflections F6 were conformably deformed with the shallower footwall units. For instance, the pinch out of the mafic protolith unit (i.e., intersection of F7 and C on Figure 16b) occurs in an area where reflection F6 is shallower (also compare the depth of F6 in Figure 16a and b). If this interpretation is valid, then the general architecture of the deeper reflection F6 can help identify areas where the hanging wall-footwall contact is shallower and within mining depths.

CONCLUSIONS

Processing of the data following a prestack DMO poststack migration approach revealed some strong reflections associated with the zinc-rich massive sulphide zones. The most prominent reflection from the ore results from the interference of thin and closely-spaced massive sulphide zones and felsic-mafic volcanic rock contacts above and below the mineralization. Other weaker reflections are also associated with zinc-rich zones but no clear reflections can be attributed to the disseminated gold zones. Contacts between metamorphosed rocks with felsic and mafic protoliths in the most altered part of the footwall also produce prominent and continuous reflections. The shallowest of these reflections can be used as a proxy for the hanging wall-footwall contact which is only locally observed on the seismic data. At depth, a series of strong and continuous reflections provide indications on the general geometry of the volcanic sequences in the area of the 3D seismic survey and can help to identify areas where the hanging wall-footwall contact is shallower and within mining depth range.